UC San Diego
UC San Diego Previously Published Works

Title

Prenatal alcohol exposure contributes to negative pregnancy outcomes by altering fetal vascular dynamics and the placental transcriptome.

Permalink

https://escholarship.org/uc/item/3v73c3sv

Journal

Alcoholism, clinical and experimental research, 46(6)

ISSN

0145-6008

Authors

Pinson, Marisa R
Tseng, Alexander M
Adams, Amy
et al.

Publication Date

2022-06-01

DOI

10.1111/acer.14846

Peer reviewed

ORIGINAL ARTICLE

ALCOHOLISM
CLINICAL & EXPERIMENTAL RESEARCH

Prenatal alcohol exposure contributes to negative pregnancy outcomes by altering fetal vascular dynamics and the placental transcriptome

Marisa R. Pinson[1] | **Alexander M. Tseng**[1] | **Amy Adams**[1] | **Tenley E. Lehman**[1] | **Karen Chung**[1] | **Jessica Gutierrez**[2] | **Kirill V. Larin**[2] | **Christina Chambers**[3,4] | **Rajesh C. Miranda**[1,5,6] | **Collaborative Initiative on Fetal Alcohol Spectrum Disorders**

[1]Department of Neuroscience and Experimental Therapeutics, Texas A&M College of Medicine, Bryan, Texas, USA

[2]Department of Biomedical Engineering, University of Houston, Houston, Texas, USA

[3]Clinical and Translational Research Institute, University of California San Diego, San Diego, California, USA

[4]Department of Pediatrics, University of California San Diego, San Diego, California, USA

[5]Women's Health in Neuroscience Program, Texas A&M University College of Medicine, Bryan, Texas, USA

[6]Interdisciplinary Program of Genetics, Texas A&M University, College Station, Texas, USA

Correspondence
Rajesh C. Miranda, Department of Neuroscience & Experimental Therapeutics, Medical Research and Education, College of Medicine, Texas A&M University Health Science Center, Building 8447 Riverside Parkway, Bryan, TX 77807-3260, USA.
Email: rmiranda@tamu.edu

Abstract

Background: Prenatal alcohol exposure (PAE) has been shown to alter fetal blood flow *in utero* and is also associated with placental insufficiency and intrauterine growth restriction (IUGR), suggesting an underlying connection between perturbed circulation and pregnancy outcomes.

Methods: Timed-pregnant C57/BL6NHsd mice, bred in-house, were exposed by gavage on gestational day 10 (GD10) to ethanol (3 g/kg) or purified water, as a control. Pulse-wave Doppler ultrasound measurements for umbilical arteries and ascending aorta were obtained post-gavage (GD12, GD14, GD18) on 2 fetuses/litter. RNA from the non-decidual (labyrinthine and junctional zone) portion of placentas was isolated and processed for RNA-seq and subsequent bioinformatic analyses, and the association between transcriptomic changes and fetal phenotypes assessed.

Results: Exposure to ethanol in pregnant mice on GD10 attenuates umbilical cord blood flow transiently during gestation, and is associated with indices of IUGR, specifically decreased fetal weight and morphometric indices of cranial growth. Moreover, RNA-seq of the fetal portion of the placenta demonstrated that this single exposure has lasting transcriptomic changes, including upregulation of *Tet3*, which is associated with spontaneous abortion. Weighted gene co-expression network analysis (WGCNA) identified erythrocyte differentiation and homeostasis as important pathways associated with improved umbilical cord blood flow as gestation progresses. WGCNA also identified sensory perception of chemical stimulus/odorant and receptor activity as important pathways associated with cranial growth.

Conclusion: Our data suggest that PAE perturbs the expression of placental genes relevant for placental hematopoiesis and environmental sensing, resulting in transient impairment of umbilical cord blood flow and, subsequently, IUGR.

KEYWORDS
intrauterine growth restriction, placenta, prenatal alcohol exposure, RNA-seq, umbilical cord blood flow

INTRODUCTION

The global prevalence of alcohol exposure during pregnancy has been estimated at 9.8% (Popova et al., 2017), while in the United States, ~8% of assessed newborn infants have blood biomarkers for third trimester prenatal alcohol exposure (Bakhireva et al., 2017; Umer et al., 2020), indicating that prenatal alcohol exposure (PAE) throughout pregnancy is common. PAE can lead to a range of developmental disabilities collectively known as Fetal Alcohol Spectrum Disorders (FASD), that are prevalent in between 1.1% and 9.8% of the school-age children in the US (May et al., 2018), while the prevalence of Fetal Alcohol Syndrome (FAS), the severe end of the FASD continuum, is estimated at a global prevalence of ~0.3% (Roozen et al., 2016). FASD is associated with a wide range of adverse infant outcomes, including neurobehavioral abnormalities as well as craniofacial dysmorphologies and intrauterine growth restriction (IUGR), which are cardinal diagnostic features for FAS (Bertrand et al., 2004; Riley et al., 2011).

Prenatal alcohol exposure has been shown to impact fetal blood flow in utero in rodent and nonhuman primate models as well as in humans (Bake et al., 2012; Gundogan et al., 2008; Iveli et al., 2007; Lo et al., 2017), suggesting one mechanism by which PAE may contribute to IUGR. The placenta may be particularly sensitive to the influences of alcohol during the transition period between the 1st and 2nd trimester, as it is during the end of the 1st trimester (gestational day [GD] 9.5 to 10.5 in mice) that chorio-allantoic fusion establishes the early fetal labyrinthine zone (Woods et al., 2018) with subsequent dilation of the spiral arteries at the start of the 2nd trimester (GD10.5 to 14.5 in mice) (Adamson et al., 2002). As the 2nd trimester progresses, extensive expansion of the labyrinthine zone occurs (De Clercq et al., 2019), and there is the potential for complications such as IUGR if this neovascularization fails to progress normally (Furuya et al., 2008).

In our previous studies in pregnant women and infants in Ukraine, we reported that PAE did result in decreased indices of growth in new-born infants (Balaraman et al., 2016), and that this outcome for affected infants was mediated, in part, by miRNA signals in maternal circulation that decreased the growth of the placenta (Tseng et al., 2019). Moreover, these miRNA signals were observed as early as the second trimester, during the early growth phase of the placenta. Although infant growth deficits are a defining feature of severe FASD, the causes are poorly understood and consequently, the impact of PAE during this critical window on placental development and blood flow in relation to fetal growth needs to be evaluated. For this reason, we interrogated the effects of PAE on fetal and placental vascular dynamics and the placental transcriptome and examined the relationship between these measurements and fetal anatomical and morphometric outcomes.

MATERIALS AND METHODS

All procedures were performed in accordance with Texas A&M Institutional Animal Care and Use Committee guidelines and approval. C57/BL6NHsd dams and male mice (Envigo) were bred in-house. All procedures were approved by the Texas A&M Institutional Animal Care and Use Committee (IACUC).

Mouse model of PAE

As we have previously published to model a single binge paradigm, EtOH, at 3g/kg (prepared from 95% Koptec – Decon Labs; Catalog#V1101, delivered in a final volume of 220 μL) or purified water, as a control, was administered by intragastric gavage on GD10 using polyethylene tubing connected to a mini pump (Harvard Apparatus 11 plus, Cat# 70-2209) set to a flow rate of 100 μl/min (Bake et al., 2012). Blood (20 μl) was collected from the tail vein using heparinized capillary tubes for the determination of blood EtOH concentrations (BEC) by gas chromatography according to our previous publications (Camarillo & Miranda, 2008; Prock & Miranda, 2007; Santillano et al., 2005). The average BEC was 112 $\pm$ 11 mg/dl. At GD18, pregnancies were terminated, fetuses delivered by laparotomy and measures of fetal weight, crown-rump length (CRL), midsagittal length (MSL) (O'Leary-Moore et al., 2010), biparietal diameter (BPD), fronto-occipital distance (FOD), and placental efficiency were obtained. Subsequently, tissue was snap-frozen in liquid nitrogen and stored at −80°C preceding RNA isolation.

Blood flow imaging

C57/BL6NHsd dams were anesthetized using isoflurane (3% to 4% for initiation of anesthesia, 1% for maintenance), and maintained supine on a temperature-controlled mouse platform (with sensors for monitoring of the maternal electrocardiogram, respiration, and core body temperature; Fuji/Visualsonics). The maternal temperature was maintained at 34 to 37°C and maternal heart rate at ~425 beats/min by adjusting the level of anesthesia. The abdomen was shaved and depilated (using Nair) to improve contact with the transducer. Prewarmed (37°C) ultrasound gel (Aquasonic, Parker Laboratories Inc.) was applied to the dam's abdomen prior to positioning the transducer. An initial scan was performed on both uterine horns to verify the number and location of all fetuses. For each pregnant dam, two fetuses (one at the end of the left uterine horn and one at the end of the right uterine horn) were selected for both pre- (GD10) and postgavage (GD12, GD14, and GD18) treatment scans. The same fetuses from each uterine horn were monitored throughout gestation. Both color and pulse wave Doppler measurements for umbilical arteries and ascending aorta were obtained using a high-frequency VEVO2100 ultrasound imaging machine coupled to an MS550D Microscan™ transducer with a center frequency of 40 MHz (Visualsonics).

Data from pulse wave Doppler imaging experiments were analyzed using the VEVO2100 measurement and analysis software (Fuji/Visualsonics) to assess Acceleration (in mm/sec^2) and Velocity Time Integral (VTI, in mm^3/s). Acceleration is defined as the change in blood flow velocity overtime from the onset of systolic forward flow to

peak velocity (Phoon & Turnbull, 2003). Acceleration can be used as a measure of cardiac output in peripheral vessels (Chang et al., 2000) in human patients and in embryonic mice studies (Phoon et al., 2000) and correlates with arterial resistance. VTI, the area under the velocity envelope (Phoon & Turnbull, 2003), is a substitute measure of cardiac stroke volume through a specific blood vessel. Acceleration and VTI measurements were obtained from the umbilical artery and fetal ascending aorta. Each data point represents measurements from one fetus from either the left or the right uterine horn in one pregnant dam (to eliminate litter and uterine position effects). The results presented are mean $\pm$ SEM for each group ($n = 5$ to 6 pregnant dams), normalized to the average baseline value for the control, pre-EtOH exposed group.

Optical coherence tomography and image analysis

Fetal imaging was performed using a swept source optical coherence tomography (SSOCT) system, which consists of a broadband laser (Santec Corporation) with a central wavelength of 1310 nm, sweep rate of 50 kHz, and axial resolution of 9.76 μm (in the air). All images were processed using Matlab, and Amira 5.4 was used to analyze and measure dimensions of GD18 fetal mouse limbs and philtrum length.

RNA isolation and RNA library preparation and sequencing

Total RNA from the nondecidual (labyrinthine with the junctional zone) portion of mouse placentas was isolated using the miRNeasy mini kit (Qiagen; Catalog # 217004). Prior to analysis, RNA quality was assessed using an Agilent TapeStation RNA assay. Total RNA concentration was quantified via Qubit Fluorometric assay, and subsequently, all samples were normalized to an equivalent starting concentration. Sequencing libraries were prepared using the TruSeq Stranded Total RNA with Ribo-Zero Library Preparation kit (Illumina). Each sample was uniquely indexed (barcoded) to allow for the pooling of all samples in a single sequencing run. Library size and quality were then assessed with an Agilent TapeStation D1000 DNA assay. Samples were normalized to ~4 nM and pooled equally. Sequencing was performed on an Illumina NovaSeq S4 Flow Cell, XP running with a 150 cycle, paired-end (2×150) sequencing run to generate approximately 50 million read pairs per sample.

Bioinformatic analysis

Raw RNA-sequence data were analyzed to identify significant differences in gene expression between the gavage control versus PAE treatment groups. All reads were evaluated and trimmed of all adapter sequences and low-quality bases using *Trimmomatic* read trimmer (Bolger et al., 2014). Using *Trimmomatic* and the corresponding adapter sequences file for Illumina, reads were scanned with a sliding window of 5, cutting when the average quality per

base drops below 20, then trimming reads at the beginning and end if base quality drops below 25, and finally dropping reads if the read length is <35. Reads were then mapped to the Mus musculus (mm10) genome assembly. Read mapping was performed using HISAT2 genomic analysis software platform version 2.1.0 (Kim et al., 2015). Transcript-wise counts were generated using HTSeq (Anders et al., 2015). Differential gene expression tests were then performed using DESeq2 software version 2.1.8.3 following the guidelines recommended by Love et al. (2014) using a "treatment" x "sex" experimental design. A total of 22,103 genes had at least one read count in at least one sample and were processed for differential expression analysis using the regularized logs of normalized gene counts derived from DESeq2. We did observe a few genes whose expression was sex-dependent (see Tables S2 and S3). However, there was only 1 gene identified as uniquely expressed in male placentas and 0 genes as uniquely expressed in female placentas. Therefore, our analyses focused on the main effect of treatment on differential gene expression. All analyses were performed on the Galaxy instance of the TAMU HPRC (https://hprcgalaxy.tamu.edu/).

Correlations were calculated using the *cor()* function in R, and partial correlations were calculated using the *ppcor* package in R (Kim, 2015). Correlation plots were created with the *corrplot* R package (Wei & Simko, 2021). The "R"-based *EnhancedVolcano* package was used to make the volcano plot (Blighe et al., 2021). Pathway analysis was conducted using *ReactomePA* (Yu & He, 2016) on differentially regulated genes (FDR adjusted p-value <0.05). *ReactomePA* utilized the KEGG database (Kanehisa et al., 2017) and the *Pathview* R package (Luo & Brouwer, 2013) to visualize differentially regulated pathways. Weighted gene co-expression network analysis (WGCNA) was conducted using the *WGCNA* R package (Langfelder & Horvath, 2008) to construct networks of relatedness and identify eigengenes, or "hub" genes, from gene expression data.

To better understand which cell types of the nondecidual zone are most sensitive to PAE on GD10, we leveraged publicly available single-cell RNA-seq (scRNA-seq) resources. We and others have reported similar analyses using cell-type-specific markers obtained from scRNA-seq studies in order to extrapolate the cell composition of tissue used in bulk RNA-seq (Jew et al., 2020; Pinson et al., 2021). Cell-cycle-associated (S and G2/M phase) gene lists were extracted from the "R" *Seurat* package (Stuart et al., 2019) and applied to our bulk RNA-seq dataset. We calculated z-scores across individual genes on the extracted gene lists and then averaged these individual gene z-scores within each sample. The average z-score of each sample was then used in 2-way ANOVA analyses (sex × treatment) completed in "R." This strategy allowed us to compare the relative expression of differentially expressed genes (e.g., housekeeping genes are more highly expressed than other cell-type-specific genes) because our interest is not in absolute expression levels but rather relative expression levels as a whole for each gene list (e.g., are all genes belonging to that class elevated or downregulated due to treatment). This process was repeated for analysis of caspase transcripts (apoptosis-related caspases, including Caspase 2 [CASP2], CASP3/6/7/8/9/10 and the inflammation-related caspases,

CASP1/4/5/11/12; Shalini et al., 2015) and transcripts for cell-type-specific marker genes (Vento-Tormo et al., 2018).

Statistical analysis

Statistical analyses were conducted using the GraphPad Prism software, version 9.2.0 for Windows. Results are expressed as the mean ± SEM. The overall group effect was analyzed for significance using two-way ANOVA with Šídák's correction for multiple comparisons post hoc testing when appropriate (i.e., following a significant group effect or given a significant interaction effect between experimental conditions in two-way ANOVA), to correct for a family-wise error rate. All statistical tests, sample sizes, and post hoc analysis are appropriately reported in the results section. A value of $p < 0.05$ was considered statistically significant, and a value of $0.1 < p < 0.05$ was considered as trending toward significance. For identification of differentially regulated genes (DRGs) in the WGCNA, differentially regulated genes were defined by meeting three different criteria: (1) unadjusted p-value <0.05, (2) large effect size (Hedge's $g > 0.8$), and (3) nonoverlapping 95% confidence intervals.

Data availability

RNA-seq expression data generated during this study are available in the NCBI/GEO database (accession number, GSE195489).

RESULTS

PAE attenuates placentally directed blood flow

We examined the effect of a single exposure to EtOH on gestational day 10 (GD10) fetal blood flow in the umbilical artery and ascending aorta, as measured by the parameter Velocity Time Integral (VTI, in mm^3/s), which measures fetal cardiac systolic output within those blood vessels (Figure 1A). Our data show that blood flow significantly increased in the ascending aorta (F (1.826, 34.69) = 5.317, $p = 0.011$; Figure 1B) and in the umbilical artery (F (1.517, 30.34) = 32.96, $p < 0.0001$; Figure 1C) over development (GD12 to GD18). While it increased ~1.2-fold in the ascending aorta, it increased ~1.8-fold in the umbilical artery over the same time. PAE did not affect VTI in the ascending aorta (F (1, 20) = 1.860, $p = 0.188$; Figure 1B), but did result in a significant "Treatment by Time" interaction effect for VTI of the umbilical artery between GD12 and GD18 (F (2, 40) = 4.592, $p = 0.016$; Figure 1C). Post hoc analysis by Šídák's multiple comparisons test identified a transient but statistically significant ~20.8% decrease in umbilical artery VTI on GD14 because of PAE (adjusted $p = 0.045$; Figure 1C).

In contrast, during this developmental period, acceleration, a measure of arterial resistance, through the ascending aorta and umbilical artery, was not changed by PAE (all p-values >0.05, Figure S1A,B). There was an increase in acceleration through the ascending aorta (F (1.682, 32.80) = 137.8, $p < 0.0001$; ~5.7-fold; Figure S1A) and umbilical artery (F (1.404, 28.09) = 19.00, $p < 0.0001$; ~2.8 fold; Figure S1B) due to gestational age.
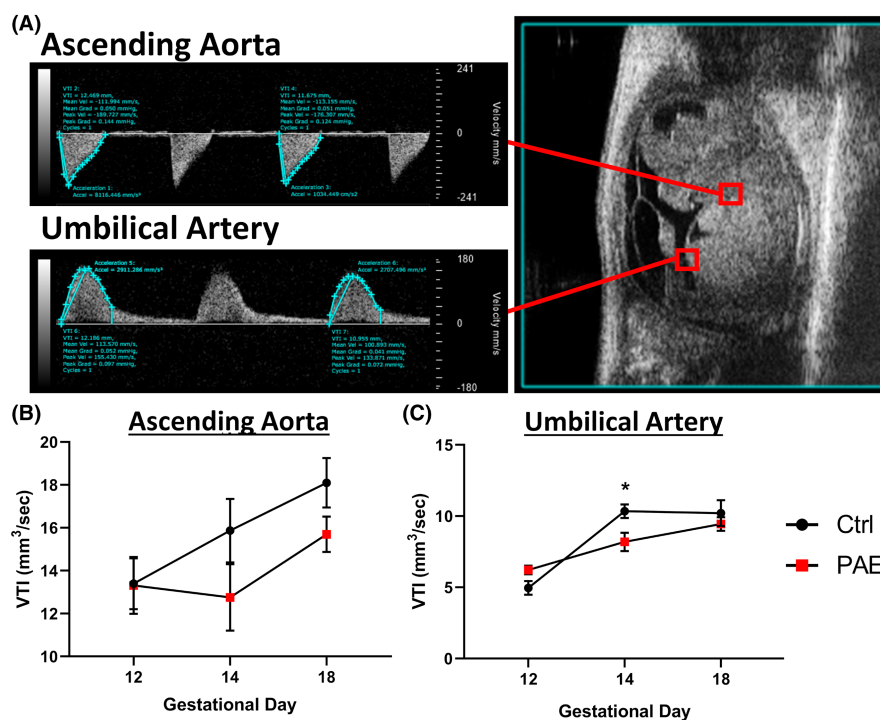

FIGURE 1 PAE transiently attenuates placentally directed blood flow. (A) Representative image of fetal mouse and measured blood flow of ascending aorta and umbilical artery. VTI of the ascending aorta (B) and umbilical artery (C) in fetal mice. VTI, Velocity Time Integral. Results are expressed as the mean ± SEM, Control $n = 12$ ($n = 6$ L), PAE $n = 10$ ($n = 5$ L). Main effect of treatment *$p < 0.05$

PAE results in fetal growth restriction

We examined the effect of a single exposure to EtOH on GD10 on fetal and placental growth by assessing growth parameters on GD18. Male and female fetuses were assessed separately, and data from all same-sex fetuses from a single pregnancy were averaged into one data point. PAE produced smaller fetuses than those in the control condition, according to all collected measures of fetal size: fetal weight (F (1, 18) = 10.58, p = 0.004; Figure 2A), crown-rump length (F (1, 18) = 3.990, p = 0.061; Figure 2D), biparietal diameter (F (1, 18) = 4.446, p = 0.049; Figure 2E), snout-occipital distance (F (1, 18) = 9.908, p = 0.006; Figure 2F), and midsagittal length (F (1, 18) = 7.196, p = 0.015; Figure 2G). Interestingly, placental weight (F (1, 18) = 2.565, p = 0.1252; Figure 2B) and placental efficiency (F (1, 18) = 0.3611, p = 0.5554; Figure 2C) were not altered in mice after a single EtOH exposure. No sex differences (all p-values >0.05) in fetal growth parameters and placental measurements were observed on GD18.

Prenatal alcohol exposure is associated with facial dysmorphology (Bertrand et al., 2004; Riley et al., 2011) and impaired long bone development (Snow & Keiver, 2007). Therefore, we were interested in determining the extent to which these FASD-associated features may be affected by a single exposure on GD10.5 as measured by philtrum length (Figure S2A) and by limb length (Figure S2C) on GD18. We observed no effect of treatment or sex on philtrum length (main effect of treatment, F (1, 11) = 2.241, p = 0.1625; main effect of sex, F (1, 11) = 1.049, p = 0.3278; Figure S2B) or limb length (main effect of treatment, F (1, 13) = 1.431, p = 0.2530; main effect of sex, F (1, 13) = 0.1417, p = 0.7127; Figure S2D).

PAE alters the relationship between blood flow and growth outcomes

We examined the relationships between fetal-placental growth parameters and blood flow dynamics by first computing Pearson's correlations without accounting for PAE (Figure 4A). Significant positive correlations were identified between GD14 VTI of the umbilical artery and fetal weight (Pearson r = 0.623, p = 0.041), snout-occipital distance (Pearson r = 0.778, p = 0.005), and frontotemporal distance (Pearson r = 0.695, p = 0.018) (Figure 3A; Figure S3A). Additionally, several significant positive relationships were identified between age-related change in VTI (ΔVTI GD12->14) of the umbilical artery and snout-occipital distance (Pearson r = 0.752, p = 0.008) and frontotemporal distance (Pearson r = 0.603, p = 0.049). Finally, significant positive correlations between litter size and GD18 VTI of the umbilical artery (Pearson r = 0.679, p = 0.022) and age-related change in VTI (ΔVTI GD14->18) of the umbilical artery (Pearson r = 0.623, p = 0.041) were identified. After correcting for PAE using partial correlation analysis, all of these significant relationships were no longer significant except for the relationship between litter size and GD18 VTI of the umbilical artery (Pearson r = 0.755, p = 0.012; Figure 3B; Figure S3B), demonstrating that PAE mediates at least

some of the relationships between placentally directed blood flow and fetal growth metrics.

PAE induces differential gene expression in the placenta

Up- and down-regulated genes were identified in nondecidual (labyrinthine with junctional zone) portions of placentas that were common to both male and female fetuses (i.e., sex-independent, males n = 6/control and n = 5/PAE, females n = 6/control and n = 5/PAE). RNA-seq analysis identified 39 significantly differentially expressed genes (DEGs; FDR-corrected p < 0.05), including 27 down-regulated genes (69.23%) and 12 upregulated genes (30.77%) (Figure 4A; Table S1). To assess for sex-specific response to PAE, DEseq2 analysis was conducted separately for male and female placentas, comparing control versus PAE for each sex. For analysis of males, 1 DEG (*Tet3*) was identified (Table S2), which was also identified in the grouped analysis. For analysis of females, no DEGs were identified (Table S3).

We also assessed whether other crucial cellular processes such as cell cycle progression and apoptosis were affected in the long term by prenatal PAE as our previous data did find an impact in an in vitro trophoblast cell model over a short time course (Tseng et al., 2019). Gene lists associated with S-phase and G2/M-phase of the cell cycle were extracted from the *Seurat* package in R. A 2-way ANOVA, comparing the averages of z-scores across all relevant genes, showed no significant difference in genes associated with S phase and G2/M (Figure S4A,B). In agreement with this, no significant difference was observed in positive and negative regulators of cell cycle progression after FDR correction (Figure S4C–H). To determine whether developmental PAE potentially influenced sensitization for apoptosis, we assessed the expression of gene transcripts associated with the execution phase of apoptosis (Fulda & Debatin, 2002; von Mering et al., 2001; Sabbagh et al., 2005), specifically the apoptosis-related caspases, including Caspase 2 (CASP2), CASP3/6/7/8/9/10, and the inflammation-related caspases, CASP1/4/5/11/12 (Shalini et al., 2015). A 2-way ANOVA, comparing the averages of z-scores across all gene transcripts belonging to these classes, showed no significant alteration in the apoptosis-related caspases (F (1, 18) = 2.381, p = 0.140) and in the inflammation-related caspases (F (1, 18) = 2.527, p = 0.129) due to PAE. We observed no main effect of sex or interaction effect between treatment and sex for the apoptosis-related caspases. For inflammation-related caspases, there was an elevation in females compared to males (F (1, 18) = 17.690, p = 0.0005; Figure S5) irrespective of treatment group, but no interaction effect between treatment and sex.

The literature suggests that PAE has the potential to alter trophoblast differentiation in vitro (Kalisch-Smith et al., 2016). Therefore, we assessed the expression of genes associated with placental cell lineages, to determine whether PAE influenced long-term maturation. We utilized publicly available single-cell RNA-seq (scRNA-seq) data (Vento-Tormo et al., 2018) to obtain gene expression patterns
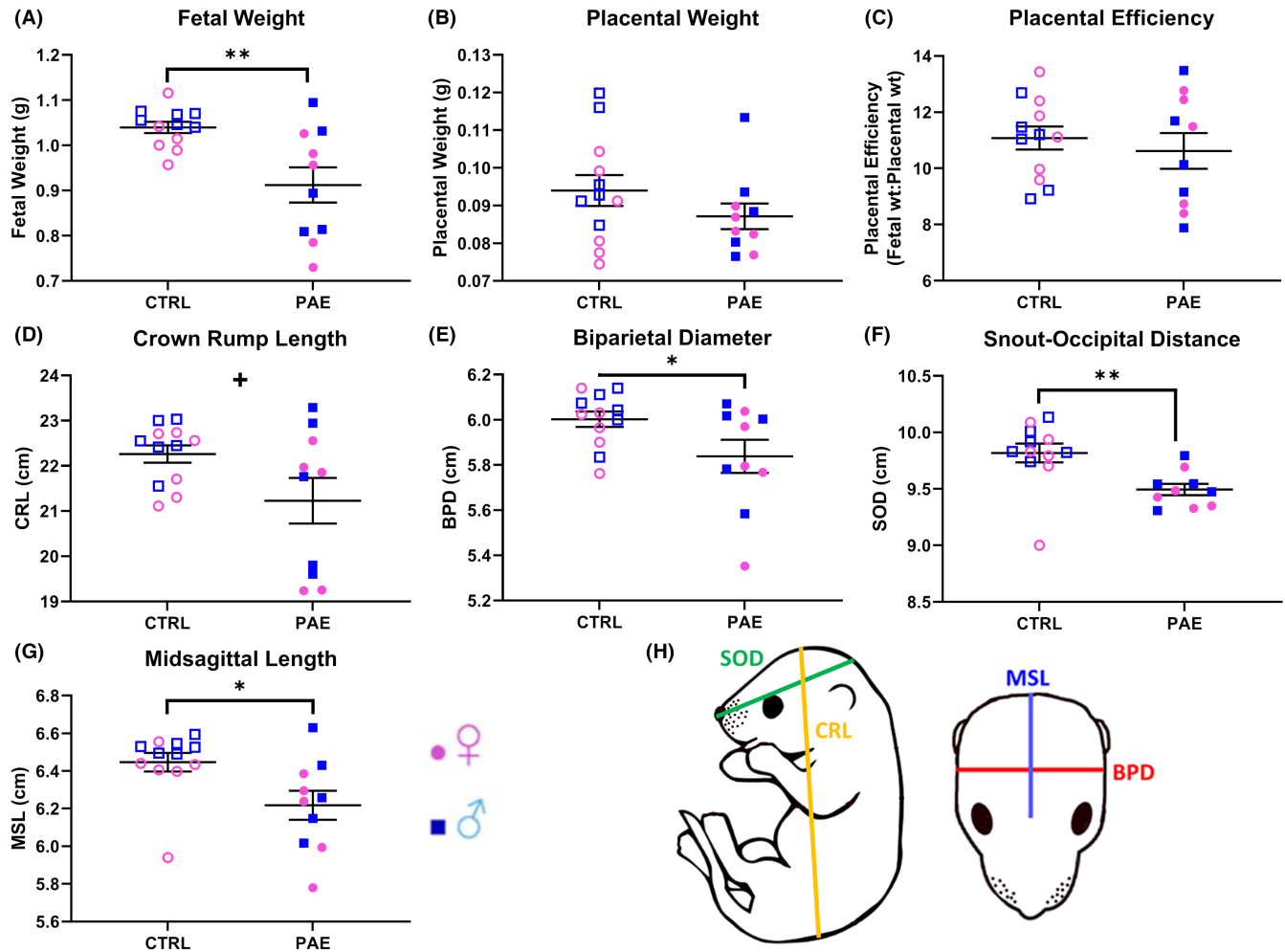
FIGURE 2 PAE restricts fetal. (A to G) Fetal weight (A), placental weight (B), placental efficiency (C), crown-rump length (D), biparietal diameter (E), snout-occipital distance (F), and midsagittal length (G) at GD18 following gavage of pregnant C57/Bl6 dams on GD10 with water (CTRL) or EtOH (PAE). (H) Schematic for measures of snout-occipital distance (SOD), crown-rump length (CRL), midsagittal length (MSL), and biparietal diameter (BPD). Dots represent median measures of fetal size and placental weights from male and female offspring in independent litters. There were no significant differences in litter sizes (Ctrl: 8.2 and PAE: 9) or sex ratios (Ctrl: 1.11 and PAE: 1.36) between treatment conditions ($p > 0.5$ for all measures). Results are expressed as the mean $\pm$ SEM, $n = 5$ to 6 separate litters per treatment condition; ANOVA: Main effect of Treatment *$p < 0.05$, **$p < 0.01$

that defined cell lineages specific to the nondecidual portion of the placenta (e.g., extravillous trophoblast, fibroblasts, Hofbauer cells, syncytiotrophoblast, and villous cytotrophoblast). However, for all nondecidual cell types assessed, we observed no main effect of treatment, the main effect of sex, nor interaction effect between treatment and sex (Table S4).

Next, we sought to identify placental gene networks that might be enriched for genes differentially regulated in the placenta on GD18 as a consequence of PAE on GD10. For this analysis, differentially regulated genes (DRGs) were defined by meeting three different criteria: (1) unadjusted p-value <0.05, (2) large effect size (Hedge's g >0.8), and (3) nonoverlapping 95% confidence intervals (482 genes, 288 down-regulated, 194 upregulated; Table S5). Using weighted gene co-expression network analysis (WGCNA), we identified 44 modules of gene networks (Table S6). Thirty-four of these 44 modules contained at least one DRG. The two modules that had DRGs as their hub genes were the *cyan* module (hub gene *Stpg4*

was down-regulated; Figure 5B) and the *darkred* module (hub gene *Vmn2r1* was down-regulated; Figure 4B). These modules also had the highest DRG enrichment scores. Gene ontology of the *cyan* module revealed genes within this network are associated with chromosome organization and nuclear processes (Figure 4C). Surprisingly, gene ontology analysis of the *darkred* module did not reveal enrichment in know pathways, suggesting that the *darkred* module may encapsulate potentially novel biological mechanisms.

Weighted gene co-expression network analysis reveals gene network modules that are correlated with the cardiac output of the umbilical artery

Because PAE resulted in a decrease in cardiac output through the umbilical artery, we conducted a correlation analysis between WGCNA module eigengenes (MEs) and fetal blood flow was
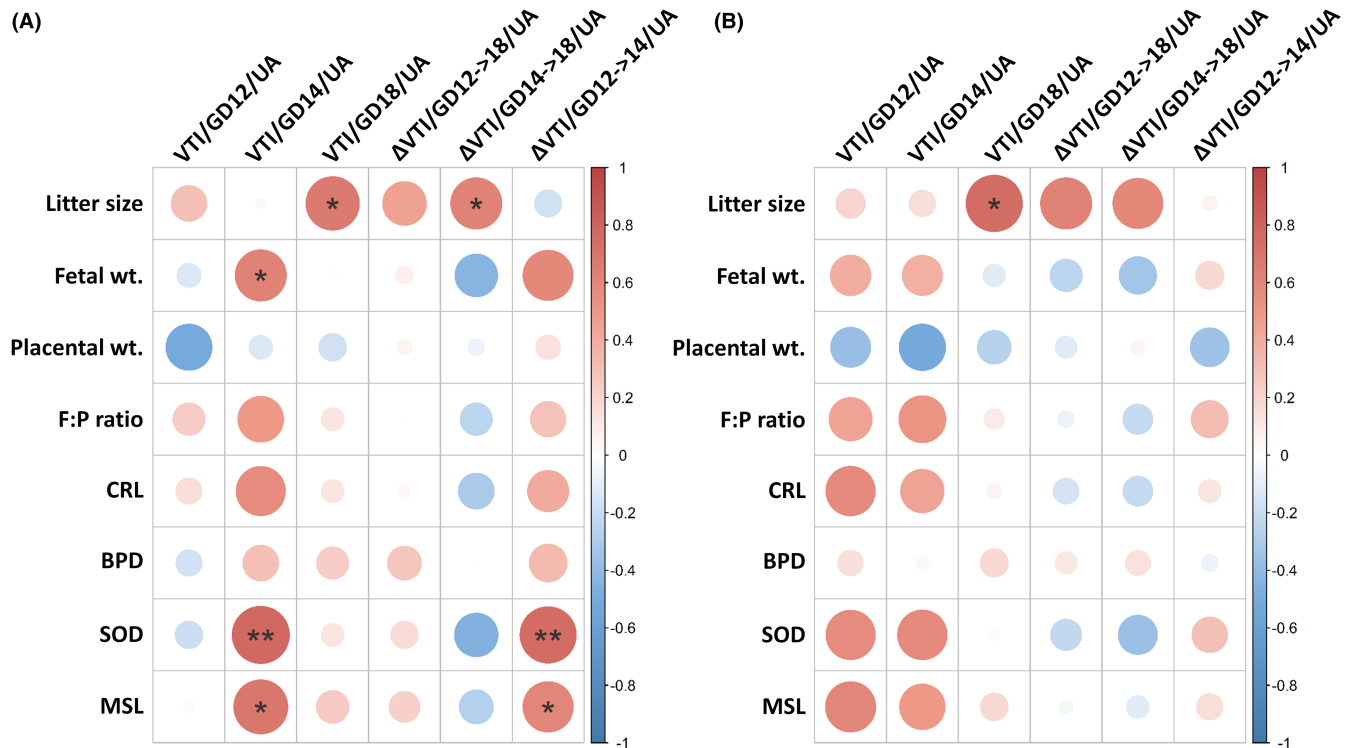
FIGURE 3 PAE alters relationship between blood flow and fetal growth outcomes. Heatmap of Pearson's correlation matrices for uncorrected analyses (A) and analyses correcting for PAE (B). For all correlation matrices, color intensity and dot size indicate a stronger correlation, with red representing a positive relationship and blue representing a negative relationship. BPD, biparietal diameter; CRL, crown-rump length; F:P ratio, placental efficiency; MSL, midsagittal length; SOD, snout-occipital distance; UA, umbilical artery; VTI, Velocity Time Integral. Control male $n = 6$, Control female $n = 6$, PAE male $n = 5$, PAE female $n = 5$. *$p < 0.05$, **$p < 0.01$

conducted (Figure 5A, Figure S6) to identify placental gene modules that were sensitive to changes in umbilical blood flow. We identified statistically significant relationships between age-related change in VTI (ΔVTI GD14->18) of the umbilical artery and the *darkred* module ($p = 0.031$) and the *paleturquoise* module ($p = 0.014$) after Benjamini-Hochberg FDR correction (Figure 5A; Figure S6). As mentioned above, the *darkred* hub gene was a DRG, *Vmn2r1*, that was down-regulated (Figure 5B), and the *darkred* module had 48 DRGs, resulting in an enrichment score of 0.2. Although the *darkred* module did not capture currently known KEGG pathways, a moderate correlation (Pearson $r = 0.47$, $p < 0.0001$; Figure S7) existed between gene significance for ΔVTI GD14->18 and gene importance in module network (Module Membership). Focusing on those genes in the top 75th percentile for module importance (Module Membership >abs(0.816)), 11 of 28 were DRGs, with 7 being down-regulated (*Vmn2r1*, *Fam20b*, *Prkcg*, *Ankdd1a*, *Adam32*, *Efcab8*, and *Tk2*) and 4 being upregulated (*Baz1a*, *Itsn2*, *Pwwp2a*, and *Zfp385c*) (Figure 5B). Gene ontology of the *paleturquoise* module identified erythrocyte differentiation and homeostasis (Figure 5C), as cellular processes that were statistically overrepresented.

Correlation analysis between WGCNA module eigengenes (MEs) and fetal blood flow also identified statistically significant relationships between GD18 VTI of the umbilical artery and the *black* module (0.007), the *purple* module ($p = 0.035$), the *grey60* module ($p = 0.029$), and the *sienna3* module ($p = 0.007$), after Benjamini-Hochberg FDR

correction (Figure 6A; Figure S6). Genes of the *black* module were associated with fatty acid metabolism (*enrichmentRatio* ranging 51 to 19.4) and fibrinolysis (*enrichmentRatio* ranging 9.7 to 18.8) (Figure S8). Genes of the *purple* module were associated with chromatin organization and nucleosome assembly (*enrichmentRatio* ranging 2.3 to 25.3; Figure S9). Genes of the *grey60* module were associated with sensory perception and receptor activity (*enrichmentRatio* ranging 3.4 to 8.6; Figure S10A). Genes of the *sienna3* module were associated with the regulation of cytokinesis and cell division (*enrichmentRatio* ranging 8.2 to 14.1; Figure S10B).

Weighted gene co-expression network analysis reveals gene network modules that are correlated with fetal growth outcomes

Prenatal alcohol exposure resulted in intrauterine growth restriction (Figure 2), and we therefore sought to identify placental gene networks that might be related to growth restriction. We identified statistically significant relationships between snout-occipital distance and the *darkgreen* module ($p = 0.003$), the *midnightblue* module ($p = 0.003$), the *paleturquoise* module ($p = 0.003$), and the *tan* module ($p = 0.02$), after Benjamini-Hochberg FDR correction (Figure 6A, Figure S11). Gene ontology analysis revealed a high degree of overlap between the *darkgreen* and *midnightblue* modules, identifying an
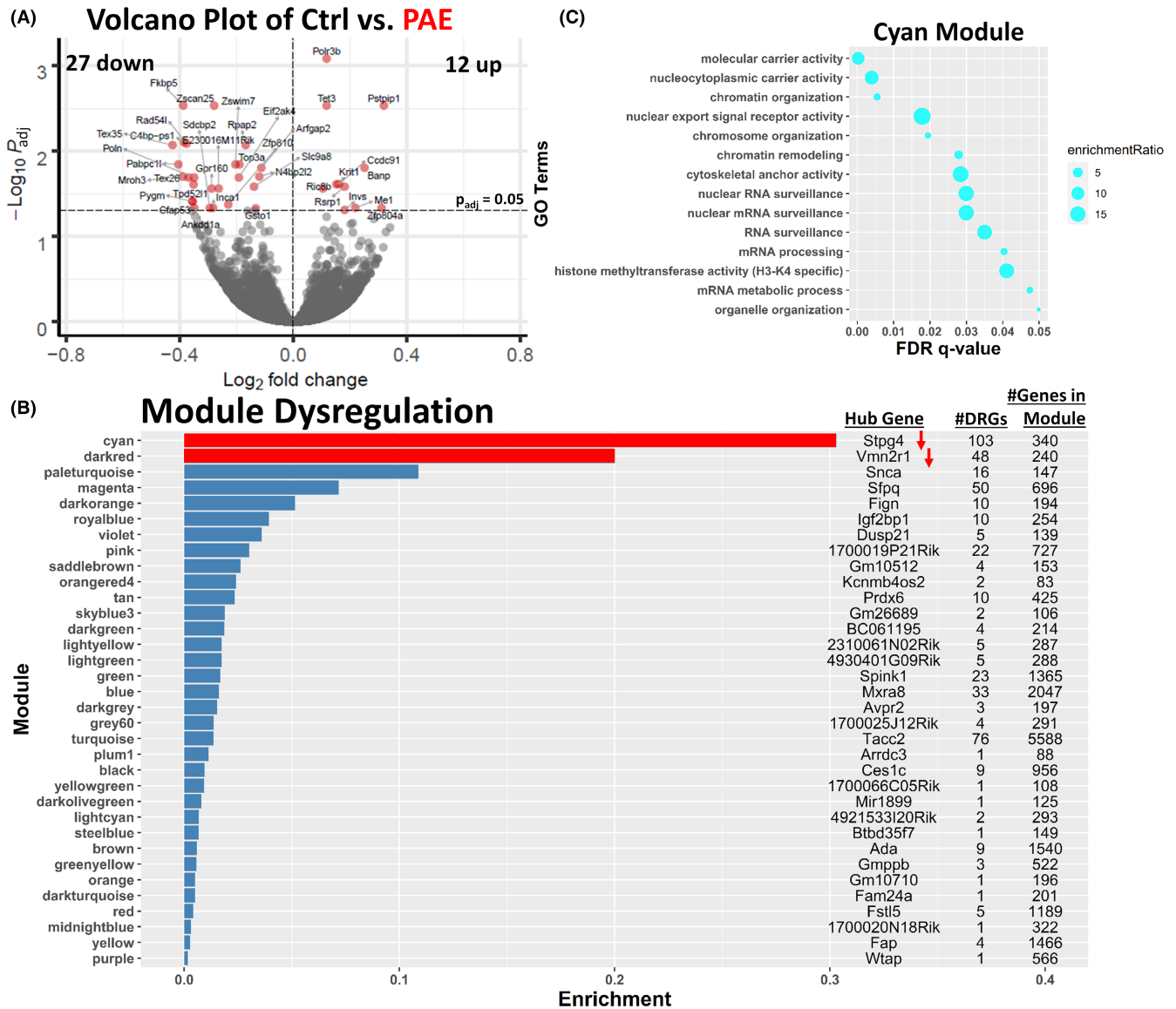
FIGURE 4 PAE results in differential gene expression and perturbation of genes of associated with chromatin organization and histone modification pathways. (A) Volcano plot of log2 fold change and −log10 *p*-value of all genes differentially expressed in placentas of control vs. PAE fetuses. (B) Bar chart showing the top PAE-dysregulated gene modules (*y*-axis). Hub gene, number of DRGs, and number of genes constituting each module are shown, with arrows indicating direction of PAE-induced expression change for each altered hub gene. Ratio of module DRGs relative to total number of genes expressed in the module is shown on *x*-axis. (C) Gene ontology (GO) analysis of *cyan* module genes focused on molecular function and biological processes. Control male *n* = 6, Control female *n* = 6, PAE male *n* = 5, PAE female *n* = 5

enrichment for sensory perception of chemical stimulus/odorant and receptor activity (Figure 6B). As mentioned previously in its relationship with ΔVTI GD14->18, the genes of the *paleturquoise* module were associated with erythrocyte differentiation and homeostasis (Figures 5C and 6B). Genes of the *tan* module were associated with cytolysis and protein mono-ADP-ribosylation (Figure 6B). Moreover, additional statistically significant relationships between the *tan* module and fetal weight (*p* = 0.048), placental efficiency (F:P ratio, *p* = 0.009), and crown-rump length (*p* = 0.003) were identified.

Relationships between the *greenyellow* module and placental efficiency (F:P ratio, *p* = 0.002) and crown-rump length (*p* = 0.002) were

also found (Figure 6A, Figure S11). Gene ontology of the *greenyellow* module identified enrichment for myoblast migration and triphosphate metabolic processes (Figure 6B, Figure S11). Finally, we also identified a statistically significant relationship between the *yellowgreen* module and biparietal diameter (*p* = 0.011; Figure 6A) and genes of this module were associated with the sensory perception of chemical stimulus/odorant and receptor activity, overlapping with the *darkgreen* and *midnightblue* modules (Figure 6B).

Gene ontology analysis was performed on all other modules, and results can be found in Tables S7 (biological processes) and 8 (molecular functions).
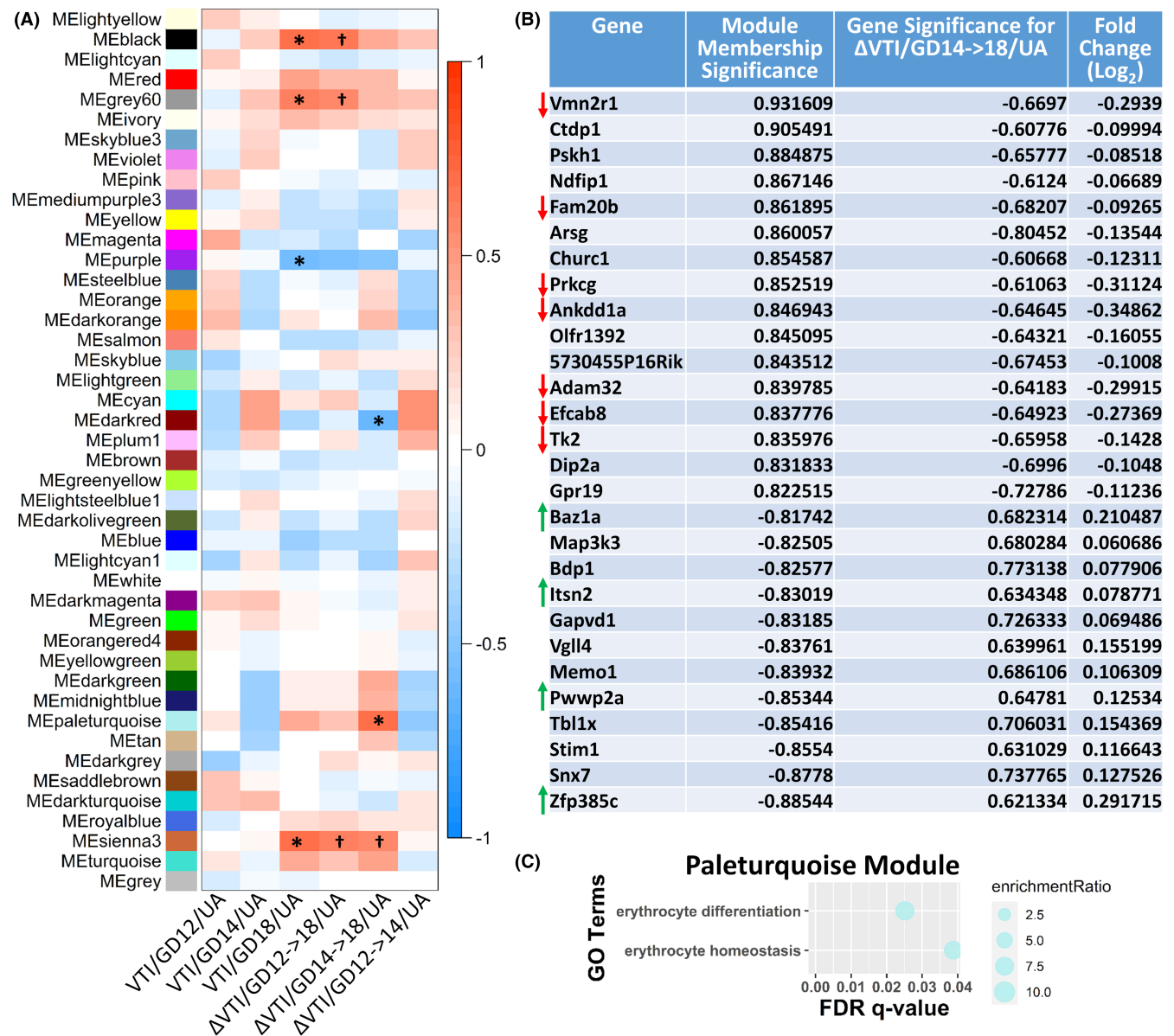
FIGURE 5 WGCNA reveals gene network associated with erythrocyte differentiation and homeostasis is related to recovery of blood flow of the umbilical artery from GD14 to GD18. (A) Heatmap of module-trait relationships depicting correlations between module eigengenes (ME) and umbilical artery VTI over time. Significant and trending correlations (Benjamini-Hochberg adjusted $p < 0.05$ and $p < 0.1$, respectively) are marked. The degree of correlation (r) is illustrated with the color legend. (B) Table listing top genes most highly associated (75th percentile) with change in VTI of umbilical artery between GD14-GD18. DRGs are marked with an arrow indicating direction of PAE-induced expression change. (C) Gene ontology (GO) analysis of *paleturquoise* module genes focused on molecular function and biological processes. UA, umbilical artery; VTI, Velocity Time Integral. Control male $n = 6$, Control female $n = 6$, PAE male $n = 5$, PAE female $n = 5$. *$p < 0.05$, †$p < 0.10$

DISCUSSION

Prenatal alcohol exposure has been shown to alter circulation in utero and to also result in IUGR (Bake et al., 2012; Gundogan et al., 2008; Iveli et al., 2007; Lo et al., 2017). Previous work in populations of pregnant women in Ukraine (Balaraman et al., 2016) and South Africa (Mahnke et al., 2021) led us to ask how placental factors may contribute to observed PAE consequences. In this study, we now report that PAE transiently but significantly impairs fetal cardiac output through the umbilical cord blood flow over gestation.

We showed that this alteration in blood flow is related to growth outcomes and that PAE mediated these relationships. Underlying these placental changes were transcriptomic changes in the fetal labyrinthine and junctional zones. While the magnitude of change in the expression levels of individual DEGs using bulk RNA-seq was relatively small, <30% using a linear scale, overall, WGCNA analysis showed a correlation in gene expression with chromatin organization and remodeling. Additional WGCNA analysis identified correlations between erythrocyte differentiation and homeostasis networks and recovery of placentally directed blood flow and
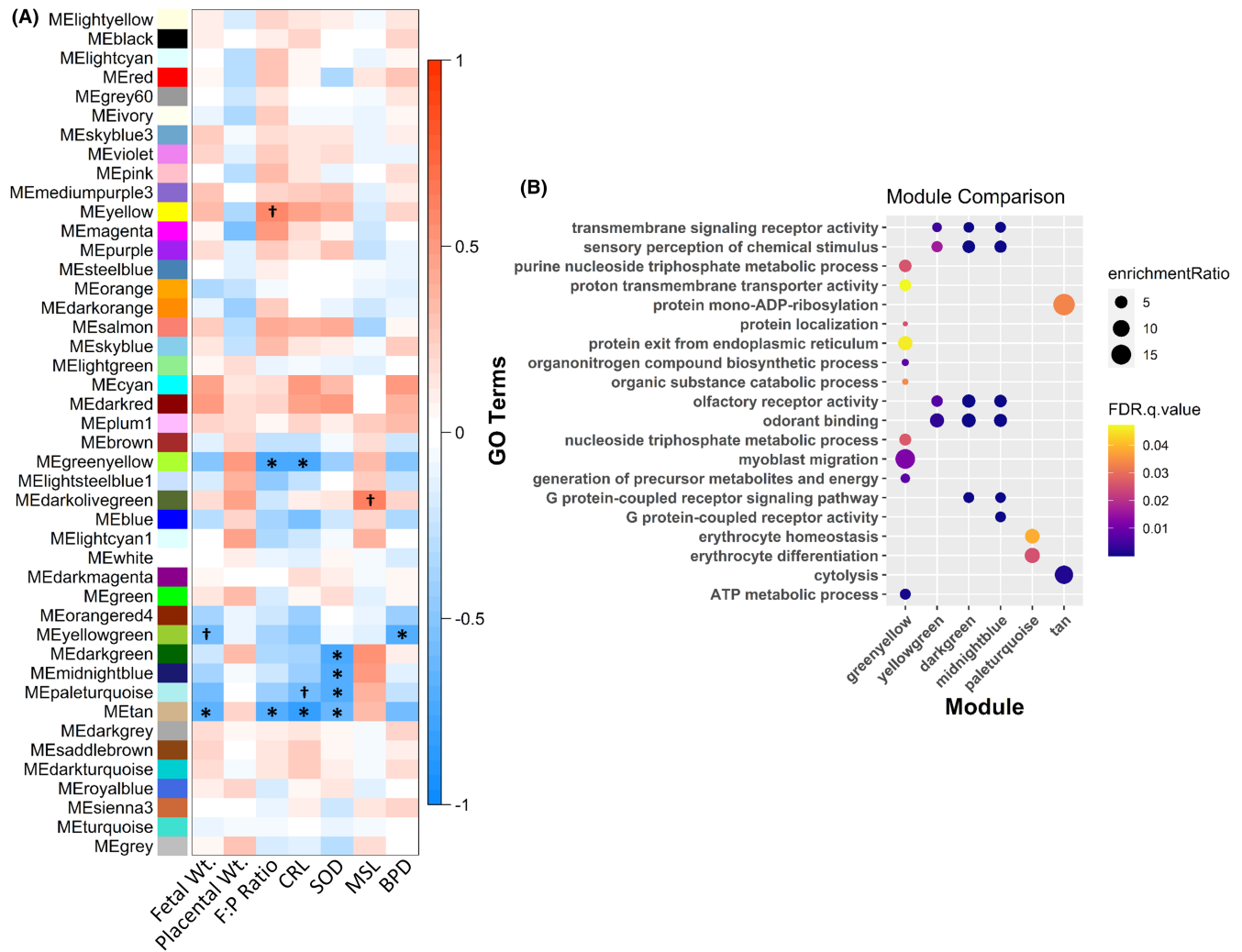
FIGURE 6 WGCNA reveals gene network associated with sensory perception of chemical/odorant and receptor activity is related to fetal head size. (A) Heatmap of module-trait relationships depicting correlations between module eigengenes (ME) and fetal-placenta growth parameters. Significant and trending correlations (Benjamini-Hochberg adjusted $p < 0.05$ and $p < 0.1$, respectively) are marked. The degree of correlation (r) is illustrated with the color legend. (B) Gene ontology (GO) analysis of genes of modules significantly correlated with fetal growth outcomes focused on molecular function and biological processes. BPD, biparietal diameter; CRL, crown-rump length; F:P ratio, placental efficiency; MSL, midsagittal length; SOD, snout-occipital distance. Control male $n = 6$, Control female $n = 6$, PAE male $n = 5$, PAE female $n = 5$. *$p < 0.05$, †$p < 0.10$

correlations between fetal growth outcomes and gene networks associated with transmembrane G protein-coupled receptor activity and odorant binding. Altogether, these data suggest that by altering placental gene expression, PAE alters placental development and subsequently umbilical artery blood flow, resulting in IUGR.

In our model, PAE occurred on GD10.5, a crucial time point during which the early fetal labyrinthine zone is established (GD9.5 to 10.5; Woods et al., 2018), with 2.5-fold dilation of the spiral arteries occurring soon after (GD10.5 to 14.5; Adamson et al., 2002). Others have shown that PAE disrupts this normal placental development, resulting in impaired trophoblast invasion and spiral artery transformation and disorganized spiral artery branching (Gundogan et al., 2008, 2013, 2015). Improper vascularization of the labyrinthine zone is associated with negative pregnancy outcomes such as pre-eclampsia and IUGR (Furuya et al., 2008), similar to what has

been shown as a consequence of PAE. In this study, we observed a decrease in umbilical cord blood flow on GD14 (mid-2nd trimester equivalent), four days after a single episode of EtOH exposure. Similar results were demonstrated in a nonhuman primate model of 1st trimester chronic exposure that measured decreased placental volume blood flow on GD110 (end of 2nd trimester equivalent), 50 days after the final EtOH exposure (Lo et al., 2017). However, the reduced umbilical cord blood flow observed in our study on GD14 proved transient, with no difference between PAE and control pregnancies observed on GD18. This recovery in umbilical artery blood flow was linked to a gene network associated with erythrocyte differentiation and homeostasis. While the direction of this relationship remains to be determined (change in blood flow results in increased erythrocyte differentiation or vice versa), others have shown that alcohol use in adults has the potential to be toxic to erythroid

precursors (Savage & Lindenbaum, 1986) and to suppress propagation of both early and late erythroid progenitor cells (Meagher et al., 1982). One study assessing differential gene expression in rat placentas on GD20 after daily EtOH exposure observed decreased expression of hemoglobin genes *Hbe1* and *Hbg1* (Rosenberg et al., 2010). Moreover, the placenta has been identified as an important loci in rodents (Alvarez-Silva et al., 2003) and humans (Van Handel et al., 2010) for hematopoietic stem cell propagation and erythropoiesis starting at the end of the first trimester (GD10.5 in mice) and peaking mid-2nd trimester (GD13.5 in mice) before diminishing as the fetal liver transitions into being the main site for these processes (Alvarez-Silva et al., 2003). The placental vascular endothelium has specifically been identified as a precursor for fetal hematopoiesis (Liang et al., 2021), which continues, albeit at lower levels as late as GD17 in the mouse (Alvarez-Silva et al., 2003), suggesting that blood flow and erythroid maturation may be functionally linked by PAE. We previously observed a link between episodic EtOH exposure and the activation of erythroid genes in neuronal lineage precursors in the fetal brain as well (Salem et al., 2021), an organ which also experiences decreased blood flow after PAE (Bake et al., 2012), suggesting that a linkage between blood flow and placental erythropoiesis represents a generalized and compensatory mechanism that requires additional investigation.

Prenatal alcohol exposure is associated with facial dysmorphology (Bertrand et al., 2004; Riley et al., 2011) and impaired long bone development (Snow & Keiver, 2007). However, we observed no impact of PAE on philtrum or forelimb development as measured on GD18 after a single exposure on GD10.5. Others have shown that the facial hypoplasia associated with Fetal Alcohol Syndrome only results from exposure during a critical window in rodents (GD7; Lipinski et al., 2012) and in nonhuman primates (GD19-20, equivalent to GD7 in the mouse; Astley et al., 1999), which is before the start of facial feature development on GD10 and formation of the mouse philtrum from fusion of the midfacial region on GD13.5 (Suzuki et al., 2016). This suggests that the cellular programming that impacts facial development was complete prior to exposure in our model. Additionally, we observed no change in fetal distal forelimb length, a growth parameter which is influenced by active chondrogenesis, which begins around GD10 in the mouse but does not peak until approximately GD15.5 (Nakamura et al., 2006; Rafipay et al., 2018). Moreover, previous studies in rodents (Snow & Keiver, 2007) and sheep (Ramadoss et al., 2006) showed impaired bone growth and ossification after chronic exposure to EtOH during the entirety of gestation. Work has not yet been done to characterize a critical window for PAE to influence bone development. This suggests that the growth of the philtrum and the distal extremities are more resilient to a single EtOH exposure than the brain and skull, as we did observe that EtOH exposure resulted in smaller cranial dimensions.

It is well documented that PAE results in persistent epigenetic alterations of chromosome methylation (Portales-Casamar et al., 2016) and circulating miRNA (Balaraman et al., 2016; Mahnke et al., 2021) in individuals with FASD. Moreover, it has also been shown that different animal models of PAE alter the epigenetic landscape

of the placenta (Kalisch-Smith et al., 2019; Loke et al., 2018) and that PAE-associated changes in circulating miRNA impairs placental development (Tseng et al., 2019). In this study, we observed an upregulation of *Tet3*, an initiator of DNA demethylation, and, for the gene network most highly enriched in DRGs, identified chromatin organization and histone modification pathways as the most highly enriched. *Tet3* induces demethylation of CpG sites and is involved in the differentiation and regulation of placental trophoblasts (Logan et al., 2013). Its expression is temporally dynamic in both the mouse and the human placenta, peaking between GD8.5 and 12.5 with broad expression across multiple cell types before having a more restricted expression pattern by GD14.5 to 18.5 (Rakoczy et al., 2017). However, if this attenuation of expression fails to occur, there is the potential for negative pregnancy outcomes as upregulation of *Tet3* in late term placentas is associated with an increased risk of spontaneous abortions (Vasconcelos et al., 2019), as has been reported for PAE (Chiodo et al., 2012; Sundermann et al., 2021). These transcriptomic changes suggesting alterations in the underlying epigenetic landscape may lead to a better understanding of the etiology of PAE in the placenta.

One group of three gene networks, composed of the *yellowgreen*, *darkgreen*, and *midnightblue* modules, exhibited consistent overlap in pathways (sensory perception of chemical stimulus/odorant and receptor activity) and were all correlated with fetal head size (e.g., SOD and BPD). Network genes identified as important in these sensing pathways were predominantly *Olfr* family genes (encoding olfactory receptors) and related genes required for olfactory receptor function and signal transduction. The expression of the *Olfr* family of genes in nonolfactory tissues is linked to chemosensation and is a means for monitoring the tissue environment. For instance, in kidneys, olfactory receptors are responsive to ligands in circulation, signaling downstream to modify renin expression and blood pressure in a mouse (Pluznick et al., 2013). The expression of *Olfr* family genes in sperm helps direct motility along chemical gradients (Spehr et al., 2003), and *Olfr* family genes have also been identified previously in the placenta of rodents (Itakura et al., 2006; Mao et al., 2010). In the rat, *Olfr* family genes were predominantly expressed in giant cell trophoblasts and spongiotrophoblast cells (Itakura et al., 2006). Moreover, placental expression of *Olfr* family genes is sensitive to maternal diet in mice (Mao et al., 2010), demonstrating that these genes are sensitive to in utero environmental changes. The relationship we identified between these chemoreception pathways and fetal head size may represent a mechanism by which the capacity to sense environmental perturbations at the placental maternal-fetal interface influences fetal growth. However, future studies will be needed to assess whether head size and placental chemosensation is causally linked or whether these are independent outcomes due to a shared exposure experience.

In conclusion, our data show that a single episode of PAE has the potential to create, in the placenta, long-lasting physiological and transcriptomic changes during development that are linked to negative fetal outcomes. A single exposure on GD10 resulted in

subsequent attenuation of umbilical cord blood flow mid-gestation (GD14). Although the index of flow, VTI, recovered by GD18, there were nevertheless persistent placental gene expression changes even at GD18. We also found that fetal weight and head size were related to alterations in blood flow dynamics and the placental transcriptome, suggesting that the placenta contributes to the underlying etiology of PAE that leads to IUGR. Our work suggests that a better understanding of these IUGR-linked and PAE sensitive pathways will provide additional perspective on PAE-induced gestational pathologies similar to what we previously found in populations of pregnant women in Ukraine and South Africa and potentially lead to effective avenues for intervention through the manipulation of compensatory pathways via epigenetic regulators such as miRNA.

CONFLICT OF INTEREST
The authors declare no conflict of interest.

ORCID
Marisa R. Pinson https://orcid.org/0000-0001-6477-9285
Christina Chambers https://orcid.org/0000-0003-4675-7722
Rajesh C. Miranda https://orcid.org/0000-0002-8359-892X

REFERENCES
Adamson, S.L., Lu, Y., Whiteley, K.J., Holmyard, D., Hemberger, M., Pfarrer, C. et al. (2002) Interactions between trophoblast cells and the maternal and fetal circulation in the mouse placenta. *Developmental Biology*, 250, 358–373.

Alvarez-Silva, M., Belo-Diabangouaya, P., Salaün, J. & Dieterlen-Lièvre, F.O. (2003) Mouse placenta is a major hematopoietic organ. *Development*, 130, 5437–5444.

Anders, S., Pyl, P.T. & Huber, W. (2015) HTSeq–a Python framework to work with high-throughput sequencing data. *Bioinformatics*, 31, 166–169.

Astley, S.J., Magnuson, S.I., Omnell, L.M. & Clarren, S.K. (1999) Fetal alcohol syndrome: changes in craniofacial form with age, cognition, and timing of ethanol exposure in the macaque. *Teratology*, 59, 163–172.

Bake, S., Tingling, J.D. & Miranda, R.C. (2012) Ethanol exposure during pregnancy persistently attenuates cranially directed blood flow in the developing fetus: evidence from ultrasound imaging in a murine second trimester equivalent model. *Alcoholism: Clinical and Experimental Research*, 36, 748–758.

Bakhireva, L.N., Sharkis, J., Shrestha, S., Miranda-Sohrabji, T.J., Williams, S. & Miranda, R.C. (2017) Prevalence of prenatal alcohol exposure in the state of Texas as assessed by phosphatidylethanol in newborn dried blood spot specimens. *Alcoholism, Clinical and Experimental Research*, 41, 1004–1011.

Balaraman, S., Schafer, J.J., Tseng, A.M., Wertelecki, W., Yevtushok, L., Zymak-Zakutnya, N. et al. (2016) Plasma miRNA profiles in pregnant women predict infant outcomes following prenatal alcohol exposure. *PLoS One*, 11, e0165081.

Bertrand, J., Floyd, R., Weber, M., O'Conner, M., Johnson, K., Riley, E. et al. (2004) *Fetal alcohol syndrome: guidelines for referral and diagnosis*. In: SERVICES, U. D. O. H. A. H. (ed.). Atlanta, GA: CDC.

Blighe, K., Rana, S. & Lewis, M. (2021) *EnhancedVolcano: publication-ready volcano plots with enhanced colouring and labeling*. R package version 1.10.0 ed.: Bioconductor.

Bolger, A.M., Lohse, M. & Usadel, B. (2014) Trimmomatic: a flexible trimmer for Illumina sequence data. *Bioinformatics*, 30, 2114–2120.

Camarillo, C. & Miranda, R.C. (2008) Ethanol exposure during neurogenesis induces persistent effects on neural maturation: evidence from an ex vivo model of fetal cerebral cortical neuroepithelial progenitor maturation. *Gene Expression*, 14, 159–171.

Chang, C.H., Chang, F.M., Yu, C.H., Liang, R.I., Ko, H.C. & Chen, H.Y. (2000) Systemic assessment of fetal hemodynamics by Doppler ultrasound. *Ultrasound in Medicine and Biology*, 26, 777–785.

Chiodo, L.M., Bailey, B.A., Sokol, R.J., Janisse, J., Delaney-Black, V. & Hannigan, J.H. (2012) Recognized spontaneous abortion in mid-pregnancy and patterns of pregnancy alcohol use. *Alcohol*, 46, 261–267.

de Clercq, K., Persoons, E., Napso, T., Luyten, C., Parac-Vogt, T.N., Sferruzzi-Perri, A.N. et al. (2019) High-resolution contrast-enhanced microCT reveals the true three-dimensional morphology of the murine placenta. *Proceedings of the National Academy of Sciences of the United States of America*, 116, 13927–13936.

Fulda, S. & Debatin, K.-M. (2002) IFNγ sensitizes for apoptosis by upregulating caspase-8 expression through the Stat1 pathway. *Oncogene*, 21, 2295–2308.

Furuya, M., Ishida, J., Inaba, S., Kasuya, Y., Kimura, S., Nemori, R. et al. (2008) Impaired placental neovascularization in mice with pregnancy-associated hypertension. *Laboratory Investigation*, 88, 416–429.

Gundogan, F., Elwood, G., Longato, L., Tong, M., Feijoo, A., Carlson, R.I. et al. (2008) Impaired placentation in fetal alcohol syndrome. *Placenta*, 29, 148–157.

Gundogan, F., Gilligan, J., Ooi, J., Sung, J., Qi, W., Naram, R. et al. (2013) Dual mechanisms of ethanol-impaired placentation: experimental mode. *Journal of Clinical and Experimental Pathology*, 3, 142.

Gundogan, F., Gilligan, J., Qi, W., Chen, E., Naram, R. & de la Monte, S.M. (2015) Dose effect of gestational ethanol exposure on placentation and fetal growth. *Placenta*, 36, 523–530.

van Handel, B., Prashad, S.L., Hassanzadeh-Kiabi, N., Huang, A., Magnusson, M., Atanassova, B. et al. (2010) The first trimester human placenta is a site for terminal maturation of primitive erythroid cells. *Blood*, 116, 3321–3330.

Itakura, S., Ohno, K., Ueki, T., Sato, K. & Kanayama, N. (2006) Expression of Golf in the rat placenta: possible implication in olfactory receptor transduction. *Placenta*, 27, 103–108.

Iveli, M.F., Morales, S., Rebolledo, A., Savietto, V., Salemme, S., Apezteguía, M. et al. (2007) Effects of light ethanol consumption during pregnancy: increased frequency of minor anomalies in the newborn and altered contractility of umbilical cord artery. *Pediatric Research*, 61, 456.

Jew, B., Alvarez, M., Rahmani, E., Miao, Z., Ko, A., Garske, K.M. et al. (2020) Accurate estimation of cell composition in bulk expression through robust integration of single-cell information. *Nature Communications*, 11, 1971.

Kalisch-Smith, J.I., Outhwaite, J.E., Simmons, D.G., Pantaleon, M. & Moritz, K.M. (2016) Alcohol exposure impairs trophoblast survival and alters subtype-specific gene expression in vitro. *Placenta*, 46, 87–91.

Kalisch-Smith, J.I., Steane, S.E., Simmons, D.G., Pantaleon, M., Anderson, S.T., Akison, L.K. et al. (2019) Periconceptional alcohol exposure causes female-specific perturbations to trophoblast

differentiation and placental formation in the rat. *Development*, 146, dev172205.

Kanehisa, M., Furumichi, M., Tanabe, M., Sato, Y. & Morishima, K. (2017) KEGG: new perspectives on genomes, pathways, diseases and drugs. *Nucleic Acids Research*, 45, D353–D361.

Kim, D., Langmead, B. & Salzberg, S.L. (2015) HISAT: a fast spliced aligner with low memory requirements. *Nature Methods*, 12, 357–360.

Kim, S. (2015) ppcor: An R package for a fast calculation to semi-partial correlation coefficients. *Communications for Statistical Applications and Methods*, 22, 665–674.

Langfelder, P. & Horvath, S. (2008) WGCNA: an R package for weighted correlation network analysis. *BMC Bioinformatics*, 9, 559.

Liang, G., Zhou, C., Jiang, X., Zhang, Y., Huang, B., Gao, S. et al. (2021) De novo generation of macrophage from placenta-derived hemogenic endothelium. *Developmental Cell*, 56, 2121–2133 e6.

Lipinski, R.J., Hammond, P., O'Leary-moore, S.K., Ament, J.J., Pecevich, S.J., Jiang, Y. et al. (2012) Ethanol-induced face-brain dysmorphology patterns are correlative and exposure-stage dependent. *PLoS One*, 7, e43067.

Lo, J.O., Schabel, M.C., Roberts, V.H.J., Wang, X., Lewandowski, K.S., Grant, K.A. et al. (2017) First trimester alcohol exposure alters placental perfusion and fetal oxygen availability affecting fetal growth and development in a non-human primate model. *American Journal of Obstetrics and Gynecology*, 216, 302.e1–302.e8.

Logan, P.C., Mitchell, M.D. & Lobie, P.E. (2013) DNA methyltransferases and TETs in the regulation of differentiation and invasiveness of extra-villous trophoblasts. *Frontiers in Genetics*, 4, 265.

Loke, Y.J., Muggli, E., Nguyen, L., Ryan, J., Saffery, R., Elliott, E.J. et al. (2018) Time- and sex-dependent associations between prenatal alcohol exposure and placental global DNA methylation. *Epigenomics*, 10, 981–991.

Love, M.I., Huber, W. & Anders, S. (2014) Moderated estimation of fold change and dispersion for RNA-seq data with DESeq2. *Genome Biology*, 15, 550.

Luo, W. & Brouwer, C. (2013) Pathview: an R/Bioconductor package for pathway-based data integration and visualization. *Bioinformatics*, 29, 1830–1831.

Mahnke, A.H., Sideridis, G.D., Salem, N.A., Tseng, A.M., Carter, R.C., Dodge, N.C. et al. (2021) Infant circulating MicroRNAs as biomarkers of effect in fetal alcohol spectrum disorders. *Scientific Reports*, 11, 1429.

Mao, J., Zhang, X., Sieli, P.T., Falduto, M.T., Torres, K.E. & Rosenfeld, C.S. (2010) Contrasting effects of different maternal diets on sexually dimorphic gene expression in the murine placenta. *Proceedings of the National Academy of Sciences of the United States of America*, 107, 5557–5562.

May, P.A., Chambers, C.D., Kalberg, W.O., Zellner, J., Feldman, H., Buckley, D. et al. (2018) Prevalence of fetal alcohol spectrum disorders in 4 US communities. *JAMA*, 319, 474–482.

Meagher, R.C., Sieber, F. & Spivak, J.L. (1982) Suppression of hematopoietic-progenitor-cell proliferation by ethanol and acetaldehyde. *New England Journal of Medicine*, 307, 845–849.

von Mering, M., Wellmer, A., Michel, U., Bunkowski, S., Tłustochowska, A., Brück, W. et al. (2001) Transcriptional regulation of caspases in experimental pneumococcal meningitis. *Brain Pathology*, 11, 282–295.

Nakamura, E., Nguyen, M.-T. & Mackem, S. (2006) Kinetics of tamoxifen-regulated Cre activity in mice using a cartilage-specific CreERT to assay temporal activity windows along the proximodistal limb skeleton. *Developmental Dynamics*, 235, 2603–2612.

O'Leary-moore, S.K., Parnell, S.E., Godin, E.A., Dehart, D.B., Ament, J.J., Khan, A.A. et al. (2010) Magnetic resonance microscopy-based analyses of the brains of normal and ethanol-exposed fetal mice. *Birth Defects Research Part A: Clinical and Molecular Teratology*, 88, 953–964.

Phoon, C.K., Aristizabal, O. & Turnbull, D.H. (2000) 40 MHz Doppler characterization of umbilical and dorsal aortic blood flow in the early mouse embryo. *Ultrasound in Medicine and Biology*, 26, 1275–1283.

Phoon, C.K. & Turnbull, D.H. (2003) Ultrasound biomicroscopy-Doppler in mouse cardiovascular development. *Physiological Genomics*, 14, 3–15.

Pinson, M.R., Holloway, K.N., Douglas, J.C., Kane, C.J.M., Miranda, R.C. & Drew, P.D. (2021) Divergent and overlapping hippocampal and cerebellar transcriptome responses following developmental ethanol exposure during the secondary neurogenic period. *Alcoholism: Clinical and Experimental Research*, 45, 1408–1423.

Pluznick, J.L., Protzko, R.J., Gevorgyan, H., Peterlin, Z., Sipos, A., Han, J. et al. (2013) Olfactory receptor responding to gut microbiota-derived signals plays a role in renin secretion and blood pressure regulation. *Proceedings of the National Academy of Sciences of the United States of America*, 110, 4410–4415.

Popova, S., Lange, S., Probst, C., Gmel, G. & Rehm, J. (2017) Estimation of national, regional, and global prevalence of alcohol use during pregnancy and fetal alcohol syndrome: a systematic review and meta-analysis. *The Lancet Global Health*, 5, e290–e299.

Portales-Casamar, E., Lussier, A.A., Jones, M.J., Macisaac, J.L., Edgar, R.D., Mah, S.M. et al. (2016) DNA methylation signature of human fetal alcohol spectrum disorder. *Epigenetics & Chromatin*, 9, 25.

Prock, T.L. & Miranda, R.C. (2007) Embryonic cerebral cortical progenitors are resistant to apoptosis, but increase expression of suicide receptor DISC-complex genes and suppress autophagy following ethanol exposure. *Alcoholism, Clinical and Experimental Research*, 31, 694–703.

Rafipay, A., Berg, A.L.R., Erskine, L. & Vargesson, N. (2018) Expression analysis of limb element markers during mouse embryonic development. *Developmental Dynamics*, 247, 1217–1226.

Rakoczy, J., Padmanabhan, N., Krzak, A.M., Kieckbusch, J., Cindrova-Davies, T. & Watson, E.D. (2017) Dynamic expression of TET1, TET2, and TET3 dioxygenases in mouse and human placentas throughout gestation. *Placenta*, 59, 46–56.

Ramadoss, J., Hogan, H.A., Given, J.C., West, J.R. & Cudd, T.A. (2006) Binge alcohol exposure during all three trimesters alters bone strength and growth in fetal sheep. *Alcohol*, 38, 185–192.

Riley, E.P., Infante, M.A. & Warren, K.R. (2011) Fetal alcohol spectrum disorders: an overview. *Neuropsychology Review*, 21, 73–80.

Roozen, S., Peters, G.J., Kok, G., Townend, D., Nijhuis, J. & Curfs, L. (2016) Worldwide prevalence of fetal alcohol spectrum disorders: a systematic literature review including meta-analysis. *Alcoholism, Clinical and Experimental Research*, 40, 18–32.

Rosenberg, M.J., Wolff, C.R., El-Emawy, A., Staples, M.C., Perrone-Bizzozero, N.I. & Savage, D.D. (2010) Effects of moderate drinking during pregnancy on placental gene expression. *Alcohol*, 44, 673–690.

Sabbagh, L., Bourbonnière, M., Sékaly, R.-P. & Cohen, L.Y. (2005) Selective up-regulation of caspase-3 gene expression following TCR engagement. *Molecular Immunology*, 42, 1345–1354.

Salem, N.A., Mahnke, A.H., Konganti, K., Hillhouse, A.E. & Miranda, R.C. (2021) Cell-type and fetal-sex-specific targets of prenatal alcohol exposure in developing mouse cerebral cortex. *iScience*, 24, 102439.

Santillano, D.R., Kumar, L.S., Prock, T.L., Camarillo, C., Tingling, J.D. & Miranda, R.C. (2005) Ethanol induces cell-cycle activity and reduces stem cell diversity to alter both regenerative capacity and differentiation potential of cerebral cortical neuroepithelial precursors. *BMC Neuroscience*, 6, 59.

Savage, D. & Lindenbaum, J. (1986) Anemia in alcoholics. *Medicine (Baltimore)*, 65, 322–338.

Shalini, S., Dorstyn, L., Dawar, S. & Kumar, S. (2015) Old, new and emerging functions of caspases. *Cell Death and Differentiation*, 22, 526–539.

Snow, M.E. & Keiver, K. (2007) Prenatal ethanol exposure disrupts the histological stages of fetal bone development. *Bone*, 41, 181–187.

Spehr, M., Gisselmann, G., Poplawski, A., Riffell, J.A., Wetzel, C.H., Zimmer, R.K. et al. (2003) Identification of a testicular odorant receptor mediating human sperm chemotaxis. *Science*, 299, 2054–2058.

Stuart, T., Butler, A., Hoffman, P., Hafemeister, C., Papalexi, E., Mauck, W.M. et al. (2019) Comprehensive integration of single-cell data. *Cell*, 177, 1888–1902.e21.

Sundermann, A.C., Velez Edwards, D.R., Slaughter, J.C., Wu, P., Jones, S.H., Torstenson, E.S. et al. (2021) Week-by-week alcohol consumption in early pregnancy and spontaneous abortion risk: a prospective cohort study. *American Journal of Obstetrics and Gynecology*, 224, 97 e1–97 e16.

Suzuki, A., Sangani, D.R., Ansari, A. & Iwata, J. (2016) Molecular mechanisms of midfacial developmental defects. *Developmental Dynamics*, 245, 276–293.

Tseng, A.M., Mahnke, A.H., Wells, A.B., Salem, N.A., Allan, A.M., Roberts, V.H. et al. (2019) Maternal circulating miRNAs that predict infant FASD outcomes influence placental maturation. *Life Science Alliance*, 2, e201800252.

Umer, A., Lilly, C., Hamilton, C., Baldwin, A., Breyel, J., Tolliver, A. et al. (2020) Prevalence of alcohol use in late pregnancy. *Pediatric Research*, 88, 312–319.

Vasconcelos, S., Ramalho, C., Marques, C.J. & Doria, S. (2019) Altered expression of epigenetic regulators and imprinted genes in human placenta and fetal tissues from second trimester spontaneous pregnancy losses. *Epigenetics*, 14, 1234–1244.

Vento-Tormo, R., Efremova, M., Botting, R.A., Turco, M.Y., Vento-Tormo, M., Meyer, K.B. et al. (2018) Single-cell reconstruction of the early maternal–fetal interface in humans. *Nature*, 563, 347–353.

Wei, T. & Simko, V. (2021) *R package 'corrplot': visualization of a correlation matrix* [Online]. Available at: https://github.com/taiyun/corrplot [Accessed 11th November 2021].

Woods, L., Perez-Garcia, V. & Hemberger, M. (2018) Regulation of placental development and its impact on fetal growth—new insights from mouse models. *Frontiers in Endocrinology*, 9, 570.

Yu, G. & He, Q.-Y. (2016) ReactomePA: an R/Bioconductor package for reactome pathway analysis and visualization. *Molecular BioSystems*, 12, 477–479.

SUPPORTING INFORMATION

Additional supporting information may be found in the online version of the article at the publisher's website.